ComTech: Computer, Mathematics and Engineering Applications, 14(2), December 2023, 101−118 P-ISSN: 2087-1244
DOI: 10.21512/comtech.v14i2.9705 E-ISSN: 2476-907X

The One-Dimensional (1D) Numerical Model: An Application to Oxygen Diffusion in Mitochondria Cell

Gandhi Napitupulu[1], Achmad Nagi[2], Mutiara Rachmat Putri[3]*, and Ivonne Milichristi Radjawane[4]

[1-4]Department of Earth Sciences, Faculty of Earth Sciences and Technology, Institut Teknologi Bandung
Jln. Ganesa No. 10, Bandung, Jawa Barat 40132, Indonesia
[3,4]Oceanography Research Group, Faculty of Earth Sciences and Technology, Institut Teknologi Bandung
Jln. Ganesa No. 10, Bandung, Jawa Barat 40132, Indonesia
[4]Korea-Indonesia Marine Technology Cooperation Research Center, Institut Teknologi Bandung
Jln. Fatahillah No.24, Cirebon, Jawa Barat 45611, Indonesia
[1]gandhinapitupulu88@gmail.com; [2]nagiachmad@gmail.com;
[3]mutiara.putri@itb.ac.id; [4]ivonnemr@itb.ac.id

Received: 6th March 2023/ **Revised:** 17th May 2023/ **Accepted:** 19th March 2023

How to Cite: Napitupulu, G., Nagi, A., Putri, M. R., & Radjawane, I. M. (2023). The One-Dimensional (1D) Numerical Model: An Application to Oxygen Diffusion in Mitochondria Cell. *ComTech: Computer, Mathematics and Engineering Applications, 14*(2), 101−118. https://doi.org/10.21512/comtech.v14i2.9705

Abstract **-** The first model of oxygen transport was formulated by August Krogh. However, the investigations conducted have yet to yield a complete analytical model and a widely applicable solution for One-Dimensional (1D) network construction. The research sought to provide numerical and analytical solutions for the oxygen transfer model in mitochondrial cells to enable researchers to estimate the molecular dynamics and diffusion characteristics in mitochondrial cells. The oxygen diffusion process in mitochondria was modeled with ID numerical models. The numerical models used to solve the equations were explicit and implicit. The explicit model consisted of Forward Time Center Space (FTCS) and DuFort-Frankel. Meanwhile, the implicit model had Crank-Nicholson and Laasonen. The numerical solutions of the explicit and implicit were divided into four scenarios with a variation of Δt and compared with the analytical solutions. The results show that the Laasonen method is the best in describing the diffusion process. The best scenario with the lowest slope value and small Root Mean Square Error (RMSE) value is scenario 2 (Δt = 3,33E-4 s and Δx = 2,00E-5 cm). The numerical model and analytical solution show that the time required to reach a steady state is 0,7 s. It indicates oxygen exchange in two sides of the mitochondrial cell after 0,7 s.

Keywords: mitochondria cell, One-Dimensional (1D) numerical model, oxygen diffusion

I. INTRODUCTION

The first model of oxygen transport was formulated by August Krogh in 1911 (Joyce & Wang, 2021). August Krogh published three important papers describing the model of oxygen (O_2) transport from capillaries to skeletal muscle, making him win the Nobel Prize in Physiology or Medicine in 1920 (Pias, 2021). For 100 years, a diffusive oxygen transport model with a partial pressure of oxygen (PO_2) profile decreasing systematically with increasing distance from the nearest capillary has been a belief in the scientific community (Damsgaard et al., 2020). However, the intervention of advances in scientific techniques, holistic experimental models, and convincing empirical data provide strong evidence against the other main tenets of Kroghian theory (i.e., capillary recruitment, the importance of intra-myocyte oxygen diffusion distance, and partial pressure of oxygen profile) (Poole, 2019). It is now known that the diffusive transport of oxygen from red blood cells in capillaries through the intravascular and interstitial spaces and into muscle cells and finally into mitochondria is more complicated than previously thought (Poole et al., 2020). These considerations provide new insights and interesting hypotheses to be tested regarding oxygen diffusion in mitochondrial cells.

An understanding of the limits of diffusion in tissues is essential to studying not only cell survival but also many forms of cellular function

*Corresponding Author

(Fathollahipour et al., 2019). Specifically, oxygen and nutrients must diffuse from the gas and liquid phases to a solid phase consisting of individual cells, groups of cells, extracellular matrix, hydrogel, or other materials to reach the cell (Figueiredo et al., 2018). Gas and nutrient levels in tissues have a significant effect on stem cell proliferation, differentiation, and overall function as it transports through various pathways, with oxygen influencing stem cell state, gene transcription, neurotransmitter metabolism, and cell viability (Salazar-Noratto et al., 2020; Shapira & Christofk, 2020; Wan et al., 2021; Wei et al., 2018).

Oxygen diffusion from the alveoli air into the pulmonary capillary blood occurs quickly (Saha & Chong, 2021). The time the red blood cells spend in the lungs near the alveolar sac is usually assumed to span between 0,2 s and 0,75 s depending on the activity of the subject (typically 0,7 s at rest) (Sikkema et al., 2022). When it reaches a cell with a low partial pressure of oxygen environment, oxygen is released from hemoglobin (Hb) and diffuses into the cell. However, not all oxygen leaves Hb. The amount released depends on tissue of partial pressure of oxygen (Juttukonda et al., 2021). In a resting state, venous blood returns to the alveolar about 75% of its oxygen content (Lanning et al., 2022). The transfer of oxygen from the alveolar air to Hb has been the subject of many theoretical, experimental, and simulation studies.

Normally, red blood cells act as a local source of O_2. In the lower panel, the Hb solution is introduced at a concentration of 70 mg/ml, with similar Hb kinetic parameters to those inside the red blood cells (Popel et al., 2003). Thus, the process of oxygen diffusion in mitochondria is modeled with One-Dimensional (1D) numerical models explicitly (Forward Time Center Space (FTCS) and DuFort-Frankel) and implicitly (Crank-Nicholson and Laasonen).

The ability to model the diffusion of oxygen into cells is an important consideration in the design of tissue constructs (Murphy et al., 2020). With the appearance of organoid culture and more complex 1D tissue models, the modeling and analysis of nutrient delivery to cells have become increasingly important. Creating diffusion models requires an understanding of complex differential equations, with a focus on numerical solutions that require specialized software and programming skills (Zhao et al., 2019). Furthermore, specific formulations are generally not available, and even when they are available, they are only applicable to certain systems and sets of conditions (Berry & Berry, 2018). General methods for solving numerically difficult differential equations were developed by Euler in the 18th century and Runge and Kutta in the 19th century. Then, many advanced methods have been and are still developed (Bailey et al., 1977). However, the investigations have not yet been made into a complete analytical model and a widely applicable solution for 1D network construction.

Therefore, the research seeks to provide a new analytical solution or closed form for the model of oxygen transfer in mitochondrial cells to enable researchers to estimate the molecular dynamics and diffusion characteristics for a particular tissue construct. This model shows derivations and solutions for several applications of differential equations. These models are then applied to mitochondrial cells to understand their characteristics and functions better. Such approaches and solutions are also broadly applicable to all types of tissue, organs, and diffusion applications, including modeling and analyzing cell function and viability in various 1D tissue constructs. It is hoped that integrating the current concepts presented in the research will provide additional encouragement and direction for research examining oxygen diffusion from red blood cells in capillaries to mitochondria, both in healthy and diseased conditions.

The researchers try to present a numerical solution for the oxygen diffusion equation in mitochondrial cells with different initial and boundary conditions. Four-time steps are performed on each numerical scheme to see the best numerical scheme. The research results are expected to describe the process of oxygen diffusion at different mitochondrial lengths and diffusion coefficients (abnormal conditions). The results of the best numerical scheme in modeling a closed 1D diffusion process are used as a basic guideline when modeling an unclosed 1D diffusion process. The best numerical scheme can be used as a first step to model oxygen diffusion in mitochondria when mitochondria are damaged (injured).

II. METHODS

The governing equation to solve the diffusion process is shown in Equation (1). This equation is diffusion one dimension at oxygen in Cartesian Coordinate. It has T as oxygen centration (mg/ml), x as space variable (cm), t as time variable (s), and a as diffusion coefficient (cm^2/s). Numerical models used to solve Equation (1) are explicit and implicit models. Explicit models consist of FTCS and DuFort-Frankel, and implicit models include Crank-Nicholson and Laasonen. The numeric solution from explicit and implicit will be compared with the analytic solution.

$$\frac{\partial T}{\partial t} = \alpha \frac{\partial^2 T}{\partial x^2} \tag{1}$$

Next, FTCS is an explicit numerical scheme. It is used to solve Parabolic Differential Partial (PDP) by forward time and central space difference method. Solving PDP equation with a finite element (FE) equation with explicit FTCS is formulated as follows. Then, the numerical scheme of FTCS from Equation (2) is shown in Figure 1.

$$\frac{T_j^{n+1} - T_j^n}{\Delta t} = \alpha \frac{T_{j+1}^n - 2T_j^n + T_{j-1}^n}{\Delta x^2} + (O\Delta t, \Delta x^2)$$
$$T_j^{n+1} = T_j^n + \frac{\alpha \Delta t}{(\Delta x)^2}\left[T_{j+1}^n - 2T_j^n + T_{j-1}^n\right] + (O\Delta t, \Delta x^2) \tag{2}$$

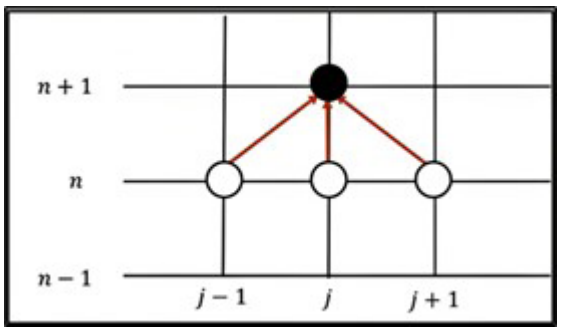

Figure 1 Numerical Scheme of Explicit Forward Time Center Space (FTCS). It has *n* as the time step and *j* as the space step.

To solve the PDP with the FE method, the researchers use the explicit DuFort-Frankel scheme. The solution is iterated at each time step by updating the solution value at a future time based on the information at the previous time step. The formula of the PDP equation with the FE equation with explicit DuFort-Frankel is shown in Equation (3). Then, the numerical scheme of DuFort-Frankel from Equation (3) is shown in Figure 2.

$$\frac{T_j^{n+1}-T_j^{n-1}}{2\Delta t}=\alpha\frac{T_{j+1}^{n}-2\frac{T_j^{n+1}+T_j^{n-1}}{2}+T_{j-1}^{n}}{\Delta x^2}+(O\Delta t^2,O\Delta x^2)$$

$$\left[1+\frac{2\alpha\Delta t}{(\Delta x)^2}\right]T_j^{n+1}=\left[1-\frac{2\alpha\Delta t}{(\Delta x)^2}\right]T_j^{n-1}+\frac{2\alpha\Delta t}{(\Delta x)^2}\left[T_{j+1}^{n}+T_{j-1}^{n}\right]+(O\Delta t^2,O\Delta x^2) \quad (3)$$

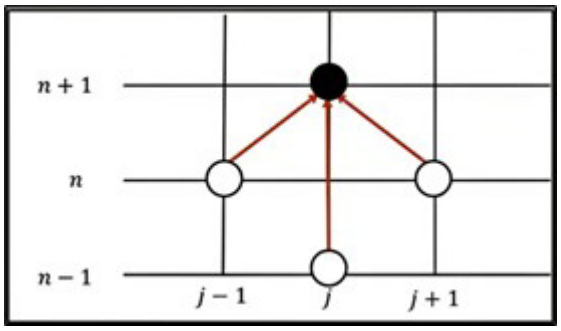

Figure 2 Numerical Scheme of Explicit DuFort-Frankel. It has *n* as the time step and *j* as the space step.

To solve the PDP by the FE method, the researchers also apply the Crank-Nicholson implicit scheme. The solution at each time step is updated by considering the information at the previous time step and according to the half-life ratio. Equation (4) shows the PDP equation with an FE equation with implicit Crank-Nicholson. Then, with $\frac{v\Delta t}{2(\Delta y)^2}=\beta$, Equation (4) can be written as Equation (5).

$$\frac{T_j^{n+1}-T_j^{n}}{\Delta t}=\frac{v}{2}\left[\frac{T_{j+1}^{n+1}-2T_j^{n+1}+T_{j-1}^{n+1}}{\Delta y^2}+\frac{T_{j+1}^{n}-2T_j^{n}+T_{j-1}^{n}}{\Delta y^2}\right]$$

$$\frac{v\Delta t}{2(\Delta y)^2}T_{j+1}^{n+1}-\left[1+\frac{v\Delta t}{(\Delta y)^2}\right]T_j^{n+1}+\frac{v\Delta t}{2(\Delta y)^2}T_{j-1}^{n+1}=-\frac{v\Delta t}{2(\Delta y)^2}T_{j+1}^{n}-\left[1-\frac{v\Delta t}{(\Delta y)^2}\right]T_j^{n}-\frac{v\Delta t}{2(\Delta y)^2}T_{j-1}^{n} \quad (4)$$

$$\beta T_{j+1}^{n+1}-(1+2\alpha)T_j^{n+1}+\beta T_{j-1}^{n+1}=-\beta T_{j+1}^{n}-[1-2\beta]T_j^{n}-\beta T_{j-1}^{n} \quad (5)$$

The linear in the matrix to solve this equation, with T_0^{n+1} and T_{jmax}^{n+1}, is boundary conditions. Gauss elimination can solve linier equation. So, the matrix can be formed in Equation (6). Then, the numeric scheme for the Crank-Nicholson method from Equation (6) is shown in Figure 3.

$$\begin{pmatrix}-(1+2\beta) & \beta & 0 & \cdots & & \\ \beta & -(1+2\beta) & \beta & \cdots & & \\ \vdots & & & \ddots & & \vdots \\ & & & \cdots & -(1+2\beta) & \beta \\ & & & & \beta & -(1+2\beta)\end{pmatrix}\begin{pmatrix}u_1^{i+1}\\ u_2^{i+1}\\ \vdots\\ u_{jmax-2}^{i+1}\\ u_{jmax-1}^{i+1}\end{pmatrix}=\begin{pmatrix}-u_1^{i}-\beta T_0^{i+1}\\ -u_2^{i}\\ \vdots\\ -u_{jmax-2}^{i}\\ -u_{jmax-1}^{i}-\beta T_{jmax}^{i+1}\end{pmatrix} \quad (6)$$

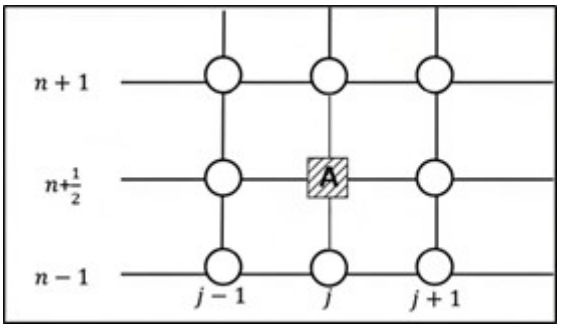

Figure 3 Numerical Form of Crank-Nicholson. It has *n* as the time step and *j* as the space step.

The Laasonen method is an explicit method with the second derivative of oxygen for space at time step $n + 1$. Solving the Partial Differential Equation (PDE) equation with the PE equation using the Laasonen method can be written in Equation (7). Then, with

$\frac{v\Delta t}{(\Delta y)^2} = \alpha$, Equation (7) can be written as Equation (8).

$$\frac{T_j^{n+1}-T_j^n}{\Delta t} = v\frac{T_{j+1}^{n+1}-2T_j^{n+1}+T_{j-1}^{n+1}}{\Delta y^2}$$

$$\frac{v\Delta t}{(\Delta y)^2}T_{j+1}^{n+1} - \left[1+2\frac{v\Delta t}{(\Delta y)^2}\right]T_j^{n+1} + \frac{v\Delta t}{(\Delta y)^2}T_{j-1}^{n+1} = -T_j^n \quad (7)$$

$$\beta T_{j+1}^{n+1} - (1+2\beta)T_j^{n+1} + \beta T_{j-1}^{n+1} = -T_j^i \quad (8)$$

Then, Equation (7) becomes a matrix to solve this equation, with T_0^{n+1} and *is* as boundary conditions. Gauss elimination is used to solve this equation. So, this matrix in Equation (9) can be formed. Then, a numeric scheme for the Laasonen method from Equation (9) can be also formed in Figure 4.

$$\begin{pmatrix} -(1+2\beta) & \beta & \cdots & & \\ \beta & -(1+2\beta) & & & \\ & & \cdots & \cdots & \beta \\ & & \cdots & \cdots & -(1+2\beta) \end{pmatrix}$$

$$\begin{pmatrix} T_1^{i+1} \\ T_2^{i+1} \\ \vdots \\ T_{jmax-2}^{i+1} \\ T_{jmax-1}^{i+1} \end{pmatrix} = \begin{pmatrix} -T_1^i - \beta T_0^{i+1} \\ -T_2^i \\ \vdots \\ -T_{jmax-2}^i \\ -T_{jmax-1}^i - \beta T_{jmax}^{i+1} \end{pmatrix} \quad (9)$$

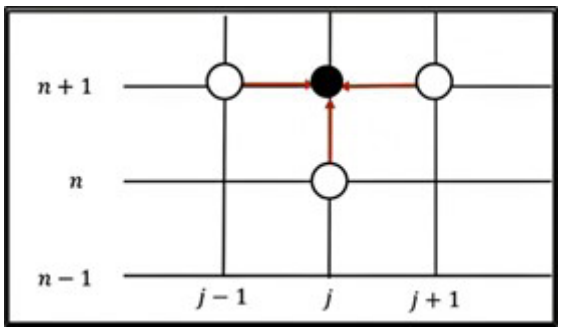

Figure 4 Numerical Form of Laasonen.
It has *n* as the time step and *j* as the space step.

Equation (1) can be solved with an analytical solution. After the analytical solution is obtained, non-homogeneous boundary conditions or non-uniform boundary conditions can be easily incorporated into the solution by specifying appropriate values on the system boundary.

$$T(0,t) = T_1\ , T(L,t) = T_2, T(x,0) = f(x) \quad (10)$$

When $T_{ss}(x)$ is in the steady state for oxygen distribution for a long time, it becomes as follows. This indicates that the oxygen distribution has reached equilibrium. There is no significant change in the elapsed time.

$$0 = \frac{\partial T_{ss}}{\partial t} - \alpha\frac{\partial^2 T_{ss}}{\partial x^2} \rightarrow \frac{\partial^2 T_{ss}}{\partial x^2} = 0 \quad (11)$$

$$T_{ss}(0) = T_1, T_{ss}(L) = T_2 \quad (12)$$

The differential equation $\frac{\partial T_{ss}}{\partial t} = 0$ produces T_{ss} to become linear equation of x (Al Mamun et al., 2018). It is $T_{ss}(x) = Ax + B$. Applying the boundary condition produces $B = T_1$ and $A = \frac{T_2-T_1}{L}$, so it obtains $T_{ss}(x) = \frac{T_2-T_1}{L}x + T_1$.

Auxiliary function is defined as $\tau(x,t)$ becoming $T(x,t) = T_{ss}(x) + \tau(x,t)$. It shows $\tau(x,t)$ is the difference between an actual solution and a steady-state solution. Equation (1) adds to the right and left sides, producing several following equations.

$$T_1 = T(0,t) = T_{ss}(0) + \tau(0,t) = T_1 + \tau(0,t) \quad (13)$$

$$T_2 = T(L,t) = T_{ss}(L) + \tau(L,t) = T_2 + \tau(L,t) \quad (14)$$

$$f(x) = T(x,0) = T_{ss}(x) + \tau(x,0) = \frac{T_2-T_1}{L}x + T_1 + \tau(x,0) \quad (15)$$

$$\tau(x,0) = f(x) - \frac{T_2-T_1}{L}x - T_1 \quad (16)$$

So, $\tau(x,t)$ qualifies $\frac{\partial \tau}{\partial t} - \alpha\frac{\partial^2 \tau}{\partial x^2} = 0$. It describes that the distribution of $\tau(x,t)$ maintains equilibrium over time and space with a rate of change in time ($\partial\tau/\partial\tau$). It is equal to the rate of oxygen diffusion in the domain.

$\tau(0, t) = 0$, $T(L, t) = 0$, $T(x, 0) = F(x)$

$$\text{with } F(x) = f(x) - \frac{T_2-T_1}{L}x - T_1 \quad (17)$$

PDE or Boundary Value Problems (BVP) is solved by applying analytical solutions. They allow modeling and solving systems with given boundary conditions. PDE/BVP is solved as follows.

$$\tau(x,t) = \sum_{n=0}^{\infty} c_n e^{-\left(\frac{\alpha n\pi}{L}\right)^2 t} \sin\left(\frac{n\pi}{L}x\right) \quad (18)$$

Then, it has $c_n = \frac{2}{L}\int_0^L F(x)\sin\left(\frac{n\pi}{L}x\right)dx$. It has c_n as a coefficient that describes the contribution of the oxygen distribution $sin(n\pi/Lx)$ in the Fourier expansion of the solution. The analytic solution for Equation (1) with the different boundary conditions is as follows.

$$T(x,t) = \frac{T_2-T_1}{L}x + T_1 + \sum_{n=0}^{\infty} c_n e^{-\left(\frac{\alpha n\pi}{L}\right)^2 t} \sin\left(\frac{n\pi}{L}x\right) \quad (19)$$

with

$$c_n = \frac{2}{L}\int_0^L \left(f(x) - \frac{T_2-T_1}{L}x - T_1\right)\sin\left(\frac{n\pi}{L}x\right)dx \quad (20)$$

The design of a numerical scheme to solve Equation (1) is as follows. A capillary vessel has a length of 1×10^{-3}cm in Figure 5 with an initial concentration of 0 mg/ml. The oxygen concentration on the right side is 70 mg/ml, and the left side is 10 mg/ml. The value of the diffusion coefficient (a) is 5,5×10-7 cm^2/s at normal blood pressure (P_B) of 100 mmHg based on laboratory results (Popel et al., 2003).

The description parameter of the numerical model shown in Table 1 with a time of simulation is 1 s. The time step of the simulation is used differently as it is divided into four categories. This category is used to see the stability of each method to solve Equation (1) with a numerical model.

After obtaining the best numerical scheme and discretization variation in modeling the oxygen diffusion process, the time course of oxygen diffusion over a range of blood pressure limits will be modeled. The range of human blood pressure in capillaries varies depending on the location of the capillaries in the body and the health condition of the individual. However, the average human blood pressure (P_B) generally ranges from 60 to 160 mmHg (Koeppen & Stanton, 2023). The effect of a change in blood pressure is considered linear to the change in the value of a.

III. RESULTS AND DISCUSSIONS

Numerical model stability is used to know the approach distribution of 1D oxygen value for the diffusion process. Stability occurs when a resulting differential equation is finite or does not blow up. Von Neumann method is used to know the stability as shown in Equation (21). Discretized is stable if it is $|\rho| < 1$.

$$T_j^n = \rho^n e^{jki\Delta x} \tag{21}$$

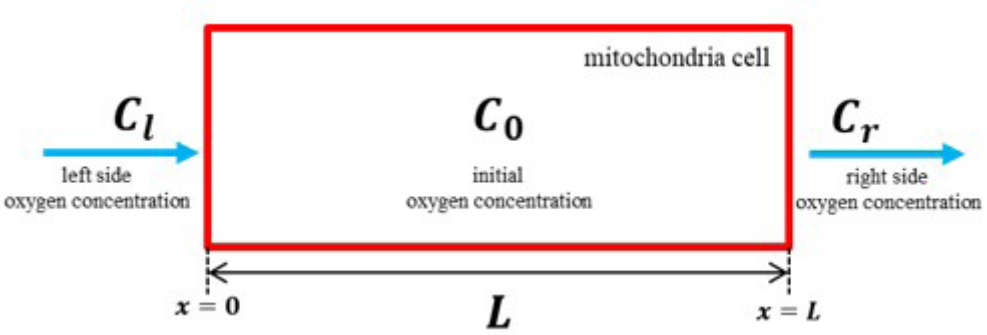

Figure 5 Simulation Scheme for the Numerical Model

Table 1 Parameter Description for Explicit and Implicit Methods

	Method	Total Grid		Δx (cm)	Δt (s)	Stability Value
		Space	Time			
Explicit	Forward Time Center Space (FTCS)	50	2000	2,00E-05	5,00E-04	0,69
			3000		3,33E-04	0,46
			3500		2,86E-04	0,39
			4000		2,50E-04	0,34
	DuFort-Frankel	50	2000	2,00E-05	5,00E-04	0,69
			3000		3,33E-04	0,46
			3500		2,86E-04	0,39
			4000		2,50E-04	0,34
Implicit	Crank-Nicolson	50	2000	2,00E-05	5,00E-04	0,69
			3000		3,33E-04	0,46
			3500		2,86E-04	0,39
			4000		2,50E-04	0,34
	Laasonen	50	2000	2,00E-05	5,00E-04	0,69
			3000		3,33E-04	0,46
			3500		2,86E-04	0,39
			4000		2,50E-04	0,34

Note: Δx and Δt are the spatial and temporal resolutions.

Stability of numerical method FTCS has a substitution of Equation (21) to Equation (2), so it produces Equation (22). Equation (22) is an important step to ensure that the method produces stable numerical solutions. Stability is about ensuring that the numerical solution does not "blow up" or become unstable as time passes.

$$\rho^{n+1}e^{jki\Delta x} - \rho^{n}e^{jki\Delta x} = \lambda\left(\rho^{n}e^{(j+1)ki\Delta x} - 2\rho^{n}e^{jki\Delta x} + \rho^{n}e^{(j-1)ki\Delta x}\right)$$
$$-1 \le 1 - 4\lambda sin^2\left(\frac{k\Delta x}{2}\right) \le 1 \quad (22)$$

Then, the value of $sin^2\left(\frac{k\Delta x}{2}\right)$ variates in range of $0 \le sin^2\left(\frac{k\Delta x}{2}\right) \le 1$. If it is $sin^2\left(\frac{k\Delta x}{2}\right) = 0$, $|\rho| = 1$ will adequate the stability conditions for value λ. However, if it is $sin^2\left(\frac{k\Delta x}{2}\right) = 1$, Equation (22) will be adequate with $0 < \lambda \le \frac{1}{2}$. So, the FTCS method is conditionally stable if it is $0 \le \lambda \le \frac{1}{2}$.

Stability of numerical method DuFort-Frankel has a substitution of Equation (21) to Equation (3). Equation (3) represents the explicit time step in the DuFort-Frankel method.

$$[1 + 2\lambda]\rho^{(n+1)}e^{jki\Delta x} = [1 - 2\lambda]\left(\rho^{(n-1)}e^{jki\Delta x}\right) + 2\lambda\left[\rho^{n}e^{(j+1)ki\Delta x} + \rho^{n}e^{(j-1)ki\Delta x}\right]$$
$$[1 + 2\lambda]\rho^2 - 4\lambda\rho\cos(k\Delta x) - [1 - 2\lambda] = 0 \quad (23)$$

Equation (23) is a quadratic equation with $a = [1 + 2\lambda]$, $b = -4\lambda\cos(k\Delta x)$, and $c = -[1 - 2\lambda]$. The solution of Equation (23) can be found using the standard quadratic formula. So, the solution of Equation (23) is as follows.

$$\rho_{1,2} = \frac{2\lambda\cos(k\Delta x) \pm \sqrt{1 - 4\lambda^2 sin^2(k\Delta x)}}{[1+2\lambda]} \quad (24)$$

The λ is always positive because of $\left|\frac{[1-2\lambda]}{[1+2\lambda]}\right| \le 1$ for every value λ. So, the DuFort-Frankel method is unconditionally stable. Therefore, this method remains stable in various situations without requiring any restrictions on the time step or space discretization.

Stability of numerical method Crank-Nicolson is with a substitution of Equation (21) to Equation (4). The value of $sin^2\left(\frac{k\Delta x}{2}\right)$ variates in the range of $0 \le sin^2\left(\frac{k\Delta x}{2}\right) \le 1$. If it is $sin^2\left(\frac{k\Delta x}{2}\right) = 0$, it will be $|\rho| = 1$. If it is $0 < sin^2\left(\frac{k\Delta x}{2}\right) \le 1$, $|\rho|$ will depend on λ. So, the Crank-Nicholson method is unconditionally stable. It can be seen in Equation (25).

$$\rho^{(n+1)}e^{jki\Delta x} - \rho^{n}e^{jki\Delta x} = \frac{1}{2}\lambda\left[\left(\rho^{(n+1)}e^{(j+1)ki\Delta x} - 2\rho^{(n+1)}e^{jki\Delta x} + \rho^{(n+1)}e^{(j-1)ki\Delta x}\right) + \left(\rho^{n}e^{(j+1)ki\Delta x} - 2\rho^{n}e^{jki\Delta x} + \rho^{n}e^{(j-1)ki\Delta x}\right)\right]$$
$$\rho = \frac{1-2\lambda\left(\sin\left(\frac{k\Delta x}{2}\right)^2\right)}{1+2\lambda\left(\sin\left(\frac{k\Delta x}{2}\right)^2\right)} \quad (25)$$

The stability of numerical method Laasonen has a substitution of Equation (21) to Equation (7). The value of $sin^2\left(\frac{k\Delta x}{2}\right)$ variates at a range of $0 \le sin^2\left(\frac{k\Delta x}{2}\right) \le 1$. If it is $sin^2\left(\frac{k\Delta x}{2}\right) = 0$, it will be $|\rho| = 1$. Then, if it is $0 < sin^2\left(\frac{k\Delta x}{2}\right) \le 1$, $|\rho|$ will depend on λ. So, the Laasonen method is unconditionally stable. It can be seen in Equation (26).

$$\rho^{(n+1)}e^{jki\Delta x} - \rho^{n}e^{jki\Delta x} = \lambda\left[\rho^{(n+1)}e^{(j+1)ki\Delta x} - 2\rho^{(n+1)}e^{jki\Delta x} \lambda + \rho^{(n+1)}e^{(j-1)ki\Delta x}\right]$$
$$\rho = \frac{1}{1+4\lambda\left(sin^2\left(\frac{k\Delta x}{2}\right)\right)} \quad (26)$$

The result of the numerical mode includes FTCS, DuFort-Frankel, Crank-Nicolson, and Laasonen. Each method is divided into four scenarios, as shown in Table 1. The results of the FTCS method are shown in Figure 6 (see Appendices). The FTCS method requires stability conditions if it is $0 < \lambda \le \frac{1}{2}$. The first scenario is unstable because of λ = 0,69. It does not satisfy the stability condition. So, the solution blows up. Scenarios 2, 3, and 4 show a stable model, and λ value satisfies the stability condition (see Table 1).

The result of DuFort-Frankel is shown in Figure 7 (see Appendices). The Dufort-Frankel method is an unconditional condition. The first scenario shows the model remains stable, although it is λ = 0,69. It is because the DuFort-Frankel method has no stability conditions. Hence, scenarios 2, 3, and 4 also show a stable model. The distribution of oxygen changes is well illustrated where the oxygen concentration is 70 g/ml on the left side of the wall. Then, it slowly decreases to the left side of the mitochondrial wall.

The result of Crank-Nicolson is shown in Figure 8 (see Appendices). This method is also an unconditional condition. The difference in time steps also does not result in significant differences in numerical solutions. All four scenarios are equally successful in describing the change in oxygen distribution that gradually decreases from the right to the left side of the wall. The absence of significant differences is also due to the unconditionally stable Crank-Nicholson method. In addition, the computational process of this method is longer because

it requires solving a tridiagonal matrix.

The next modeling also uses four scenarios with different time steps. Although there is a considerable difference in time steps between the four scenarios, the curves show no difference. The difference occurs at the beginning of the simulation. There is a spike (the value is small). It is an advantage possessed by the implicit method. The method is unconditionally stable, so it does not depend on the selection of the magnitude of the time step that must be used to meet the stability conditions like the previous explicit method.

The simulation results with the Laasonen method can be seen in Figure 9 (see Appendices). Scenarios using four different time steps are also applied to this method. However, as can be seen, there is no significant difference in the results obtained.

A comparison of oxygen diffusion contours is shown in Figure 10 (see Appendices) using the explicit FTCS method in scenarios 1 and 4. In Figure 10A (see Appendices), the simulation stops at 0,8 s because the oxygen concentration value is getting bigger (blow up). Meanwhile, in Figure 10B (see Appendices), the simulation proceeds well because it qualifies the stability requirements.

A comparison of oxygen diffusion contours using the explicit DuFort-Frankel method in scenarios 1 and 4 is shown in Figure 11 (see Appendices). In Figure 11A (see Appendices) in scenario 1, the simulation continues, but the value is smaller than the value of scenario 4 (Figure 11B (see Appendices)). it is due to the difference in the speed of convergence. The large difference in the value of Δt results in a difference in the speed of convergence of the oxygen diffusion value.

Figure 12 (see Appendices) compares oxygen diffusion contours using the implicit Crank-Nicolson method in scenarios 1 and 4. In Figure 12A (see Appendices) in scenario 1, the simulation progresses, but the value has a spike at the beginning of the simulation. The approach uses large Δt, so it takes time to adjust. Scenario 4 (Figure 12B (see Appendices)) is good because it uses a smaller Δt. The large difference in the value of Δt results in a difference in the speed of convergence of the oxygen diffusion value.

The comparison of oxygen diffusion contours in Figure 13 (see Appendices) uses the implicit Laasonen method in scenarios 1 and 4, producing almost the same results. The convergence speed is also the same at 0,7 s. Thus, the Laasonen method produces the best simulation results to perform despite the large stability value (Table 1). The large difference in Δt value does not result in a difference in the speed of convergence of the oxygen diffusion value.

The diffusion equation is a PDE that describes density fluctuations in a material undergoing diffusion (Vázquez, 2017). Comparison of oxygen diffusion contours in Figure 14 (see Appendices) uses the analytic solution in scenarios 1 and 4. In Figure 14A (see Appendices) in scenario 1, the simulation progresses. However, the value has a spike at the beginning of the simulation because the approach uses large Δt, so it takes time to adjust. Meanwhile, scenario 4 (Figure 14B (see Appendices)) is good because it uses a smaller Δt. The large difference in the value of Δt also results in a difference in the speed of convergence of the oxygen diffusion value.

Numerical methods will always succeed in finding roots (solutions) when they meet the stability conditions of each method. However, the speed of convergence is different for each method. The speed of convergence can be increased if the value of Δt is smaller. The fastest converging method is the implicit method. In general, the solution with the tridiagonal matrix converges. The intersection points of the tangent lines of the functions quickly move closer to the true roots. The analytical solution also converges immediately in scenario 1 with Δt = 0,0005 s taking 0,0005 s to converge (Figure 15A (see Appendices)) and scenario 4 with Δt = 0,00025 s converges at 0,00025 s (Figure 15B (see Appendices)).

A comparison between the numerical solutions of each scheme has been made. Inspection of Figure 16 (see Appendices) shows that the size of the average error obtained is closely related to the size of the dominant error term in the method used. The error values are smaller for the implicit method than for the explicit method. The implicit method can adapt the forward time equation (explicit method) to the reverse time equation by only considering that all outgoing and incoming fluxes occur at $t + \Delta t$. The numerical scheme, where N is the number of cells in the domain, is more difficult to solve because it has $N + 2$ unknowns. The boundary conditions provide the other two missing equations. The time forward (explicit method) scheme is simpler as it is one equation for one unknown. The time backward scheme describes the tridiagonal matrix system in the Crank-Nicolson and Laasonen schemes. Such systems can be solved using the Gauss-Seidel elimination method or, more efficiently, the Thomas algorithm. The advantage is that the implicit always exhibits a solution value that is always stable. In this project, the researchers discuss finite difference methods for diffusion problems in 1D. The researchers analyze the solutions of the C approximation. It can be concluded that the method performs well for large values. The researchers also present some analytical behavior of the problem that explains the presence of oscillations in the approximated solution for small values of Δt (Figures 16C and 16D (see Appendices)).

The Central Processing Unit (CPU) time required to run with a given value of Δt depends on the value of Δt used, and this time increases as length of Mitochondria cell (L) increases. Moreover, there is a difference in the CPU time required by the explicit and implicit methods. Implicit methods are about 1,3 longer than the explicit methods. Moreover, a numerical method based on the approach used requires much less computational effort. When the results obtained for the explicit formula are compared with those of the implicit scheme, the average error of the former is generally found to be about two orders of magnitude greater than the latter.

Next, the researchers have compared four methods for the solution of diffusion problems in 1D. The results show that the Laasonen method is the best in describing the diffusion process. The fundamental reason lies in the numerical discretization of each method, so there is no bias in the Laasonen method from the beginning of the scheme to the steady state. Meanwhile, in the Crank-Nicholson method, as seen in Figures 12 (see Appendices) and 13 (see Appendices), there is a spike at the beginning of the scheme because the numerical method solves the problem.

The scenarios of the Laasonen method are divided into four categories in Table 1. The comparison of the results of the analytic solution with the Laasonen scheme is shown in Figure 17 (see Appendices). The slope value of the graph and RMSE can be seen in Table 2. The best scenario with the lowest slope value and small RMSE value is scenario 2 ($\Delta t = 3{,}33E-04$s and $\Delta x = 2{,}00E-05$s). The error value in the scenario (Figure 16A (see Appendices)) is also the closest to the value of 0 mg/ml.

Table 2 Slope Value and RMSE of the Analytic Solution and Laasonen Method

Method	Scenario	Slope	Root Mean Square Error (RMSE) (mg/ml)
Laasonen	1	1.018	2.880
	2	1.018	2.875
	3	1.041	1.904
	4	1.036	2.121

Numerical models for oxygen diffusion are usually based on PDE. Four discretization methods are used to solve these equations numerically, namely FTCS, DuFort-Frankel, Crank-Nicolson, and Laasonen. The researchers also need to consider appropriate boundary conditions and initial conditions, such as initial oxygen concentration, oxygen concentration around the membrane, and the rate of oxygen supplied or taken up by the tissue, referring to laboratory results that have been conducted (Popel et al., 2003). The simulation results show that the best discretization method is the Laasonen Method.

The Laasonen method is an implicit numerical method that combines the forward Euler time scheme and the central space scheme to calculate oxygen transfer in lung tissue. In this method, time is updated at each iteration step using the forward Euler scheme, while oxygen displacement is calculated using the central scheme. This method has advantages in numerical accuracy and stability, as well as fast convergence time (Figures 16 and 17 (see Appendices)). The time required in the diffusion process (T_D) of oxygen is 0,7 s. This result is in accordance with laboratory results conducted previously on the oxygen diffusion process in mitochondrial cells under normal circumstances (P_B = 100 mmHg) (Sikkema et al., 2022). Oxygen diffusion time in human blood pressure variations in the blood pressure range (P_B) 60−180 mmHg can be seen in Table 3.

Table 3 Oxygen Diffusion Time at Varying Human Blood Pressure

(mmHg)	(cm^2/s)	(s)
60	$3{,}3 \times 10^{-7}$	1,20
80	$4{,}4 \times 10^{-7}$	0,90
100	$5{,}5 \times 10^{-7}$	0,70
120	$6{,}6 \times 10^{-7}$	0,55
140	$7{,}7 \times 10^{-7}$	0,48
160	$8{,}8 \times 10^{-7}$	0,42

Note: blood pressure range (P_B), diffusion coefficient (a), and the time required in the diffusion process (T_D).

IV. CONCLUSIONS

Implementation of explicit and implicit finite element methods for oxygen diffusion has been carried out and validated with analytical solutions. The researchers have presented numerical solutions with exact solutions for the oxygen diffusion equation in mitochondrial cells with different initial conditions and boundary conditions. The numerical methods used are explicit schemes (FTCS and DuFort-Frankel) and implicit schemes (Crank-Nicolson and Laasonen). The researchers apply simulation parameter values that refer to laboratory calculations for diffusion in mitochondria with a simulation duration of 1 s. Four different time steps are performed for each numerical scheme to see the best numerical scheme. Simulations with explicit schemes (FTCS and DuFort-Frankel) are faster than implicit schemes (Crank-Nicolson and Laasonen) in terms of solving time. However, relative error calculations for the four different numerical schemes show that the implicit scheme exhibits a better convergence rate than the explicit scheme. The implicit scheme also does not require stability conditions. Simulation results show that the Laasonen scheme best describes the oxygen diffusion process. The best scenario is that if the slope value is close to 1, and the RMSE value is small, like in scenario 2 ($\Delta t = 3{,}33E^{-4}$ s and $\Delta x = 2{,}00E^{-5}$ cm). The numerical model and analytical solution show that the time required to reach a steady state is 0,7 s. It indicates oxygen exchange in two sides of the mitochondrial cell after 0,7 s. These results can be utilized for preliminary studies to describe the oxygen diffusion process at different (abnormal) mitochondrial lengths or diffusion coefficients. The best numerical scheme can be used to estimate the time for oxygen exchange when the mitochondrial length is abnormal. The Laasonen method can be developed to research the phenomenon of oxygen diffusion further when abnormalities occur in mitochondrial cells.

Nevertheless, the model is limited to only being used in one dimension. Therefore, for further research, additional modeling is needed to expand into three dimensions. It is necessary to accommodate more complex and in-depth aspects that may exist within a three-dimensional environment. In addition, further research can modify the initial conditions and boundary conditions in the numerical model to learn more about the factors that affect oxygen diffusion. For example, it can consider changes in mitochondrial air temperature and pressure to see the impact on oxygen transfer time.

ACKNOWLEDGEMENT

The research is part of projects titled "*Korea-Indonesia Marine Technology Cooperation Research Center* (20220512)" and "*Ocean and Coastal Basic Survey and Capacity Enhancement in Cirebon, Indonesia* (PG53340)" which are funded by the Ministry of Oceans and Fisheries, Korea.

REFERENCES

Al Mamun, A., Ali, M. S., & Miah, M. M. (2018). A study on an analytic solution 1D heat equation of a parabolic partial differential equation and implement in computer programming. *International Journal of Scientific & Engineering Research*, *9*(9), 913–921.

Bailey, D. F. (1977). Review of elementary differential equations and boundary value problems; Differential equations and their applications, an introduction to applied mathematics, by W. E. Boyce, R. C. DiPrima, & M. Braun. *The American Mathematical Monthly*, *84*(8), 664–665. https://doi.org/10.2307/2321040

Berry, F. S., & Berry, W. D. (2018). Innovation and diffusion models in policy research. In *Theories of the policy process*. Routledge. https://doi.org/10.4324/9780429494284-8

Damsgaard, C., Lauridsen, H., Harter, T. S., Kwan, G. T., Thomsen, J. S., Funder, A. M., ... & Brauner, C. J. (2020). A novel acidification mechanism for greatly enhanced oxygen supply to the fish retina. *eLife*, *9,* 1–20. https://doi.org/10.7554/ELIFE.58995

Fathollahipour, S., Patil, P. S., & Leipzig, N. D. (2019). Oxygen regulation in development: Lessons from embryogenesis towards tissue engineering. *Cells Tissues Organs*, 205 (5–6), 350–371. https://doi.org/10.1159/000493162

Figueiredo, L., Pace, R., D'Arros, C., Réthoré, G., Guicheux, J., Le Visage, C., & Weiss, P. (2018). Assessing glucose and oxygen diffusion in hydrogels for the rational design of 3D stem cell scaffolds in regenerative medicine. *Journal of Tissue Engineering and Regenerative Medicine*, *12*(5). https://doi.org/10.1002/term.2656

Joyce, W., & Wang, T. (2021). How cardiac output is regulated: August Krogh's proto-Guytonian understanding of the importance of venous return. *Comparative Biochemistry and Physiology Part A: Molecular & Integrative Physiology, 253*. https://doi.org/10.1016/j.cbpa.2020.110861

Juttukonda, M. R., Donahue, M. J., Waddle, S. L., Davis, L. T., Lee, C. A., Patel, N. J., ... & Jordan, L. C. (2021). Reduced oxygen extraction efficiency in sickle cell anemia patients with evidence of cerebral capillary shunting. *Journal of Cerebral Blood Flow & Metabolism*, *41*(3), 546–560. https://doi.org/10.1177/0271678X20913123

Koeppen, B. M., & Stanton, B. A. (2023). *Berne and Levy physiology e-book*. Elsevier Health Sciences.

Lanning, K. M., Erkinaro, T. M., Ohtonen, P. P., Vakkala, M. A., Liisanantti, J. H., Ylikauma, L. A., & Kaakinen, T. I. (2022). Accuracy, precision, and trending ability of perioperative central venous oxygen saturation compared to mixed venous oxygen saturation in unselected cardiac surgical patients. *Journal of Cardiothoracic and Vascular Anesthesia*, *36*(7), 1995–2001. https://doi.org/10.1053/j.jvca.2021.08.103

Murphy, S. V., De Coppi, P., & Atala, A. (2020). Opportunities and challenges of translational 3D bioprinting. *Nature Biomedical Engineering, 4,* 370–380. https://doi.org/10.1038/s41551-019-0471-7

Pias, S. C. (2021). How does oxygen diffuse from capillaries to tissue mitochondria? Barriers and pathways. *The Journal of Physiology, 599*(6), 1769–1782. https://doi.org/10.1113/JP278815

Poole, D. C. (2019). Edward F. Adolph Distinguished Lecture. Contemporary model of muscle microcirculation: Gateway to function and dysfunction. *Journal of Applied Physiology, 127*(4). 1012–1033. https://doi.org/10.1152/japplphysiol.00013.2019

Poole, D. C., Pittman, R. N., Musch, T. I., & Østergaard, L. (2020). August Krogh's theory of muscle microvascular control and oxygen delivery: A paradigm shift based on new data. *The Journal of Physiology 598*(20), 4473–4507. https://doi.org/10.1113/JP279223

Popel, A. S., Goldman, D., & Vadapalli, A. (2003). Modeling of oxygen diffusion from the blood vessels to intracellular organelles. In *Oxygen transport to tissue XXIV. Advances in experimental medicine and biology*. Springer. https://doi.org/10.1007/978-1-4615-0075-9_46

Saha, B. K., & Chong, W. H. (2021). Diffuse Alveolar Hemorrhage in cardiac diseases. *Lung, 199,* 103–112. https://doi.org/10.1007/s00408-021-00433-x

Salazar-Noratto, G. E., Luo, G., Denoeud, C., Padrona, M., Moya, A., Bensidhoum, M., ... & Petite, H. (2020). Understanding and leveraging cell metabolism to enhance mesenchymal stem cell transplantation survival in tissue engineering and regenerative medicine applications. *Stem Cells, 38*(1), 22–33. https://doi.org/10.1002/stem.3079

Shapira, S. N., & Christofk, H. R. (2020). Metabolic regulation of tissue stem cells. *Trends in Cell Biology, 30*(7), 566–576. https://doi.org/10.1016/j.tcb.2020.04.004

Sikkema, L., Strobl, D. C., Zappia, L., Madissoon, E., Markov, N. S., Zaragosi, L. E., ... & Theis, F. J. (2022). An integrated cell atlas of the human lung in

health and disease. *bioRxiv*.

Vázquez, J. L. (2017). The mathematical theories of diffusion: Nonlinear and fractional diffusion. In M. Bonforte & G. Grillo (Eds.), *Nonlocal and nonlinear diffusions and interactions: New methods and directions.* Springer. https://doi.org/10.1007/978-3-319-61494-6_5

Wan, X., Liu, Z., & Li, L. (2021). Manipulation of stem cells fates: The master and multifaceted roles of biophysical cues of biomaterials. *Advanced Functional Materials, 31*(23). https://doi.org/10.1002/adfm.202010626

Wei, P., Dove, K. K., Bensard, C., Schell, J. C., & Rutter, J. (2018). The force is strong with this one: Metabolism (over)powers stem cell fate. *Trends in Cell Biology*, *28*(7), 551–559. https://doi.org/10.1016/j.tcb.2018.02.007

Zhao, W., Cheng, Y., Pan, Z., Wang, K., & Liu, S. (2019). Gas diffusion in coal particles: A review of mathematical models and their applications. *Fuel, 252*(September), 77–100. https://doi.org/10.1016/j.fuel.2019.04.065

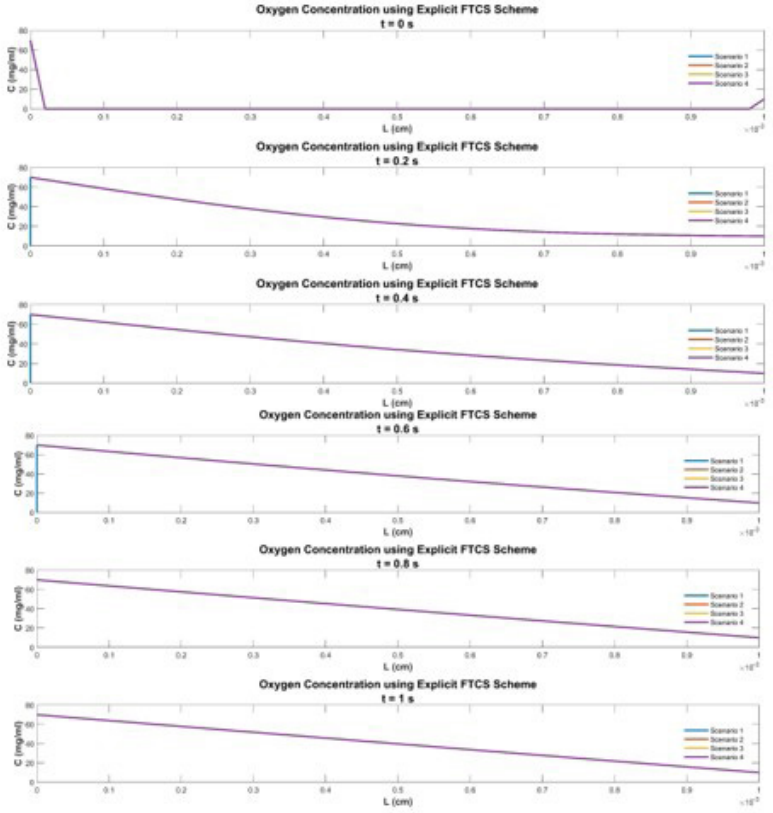

Figure 6 Simulation Results of Oxygen Diffusion with Forward Time Center Space (FTCS) method in Scenario 1 to Scenario 4

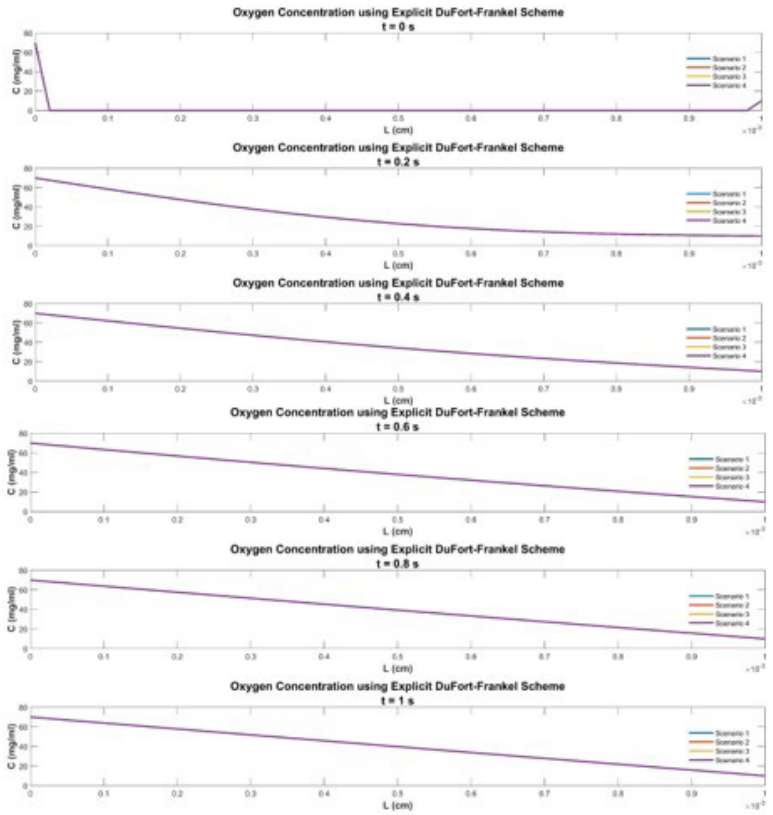

Figure 7 Simulation Results of Oxygen Diffusion with DuFort-Frankel Method in Scenario 1 to Scenario 4

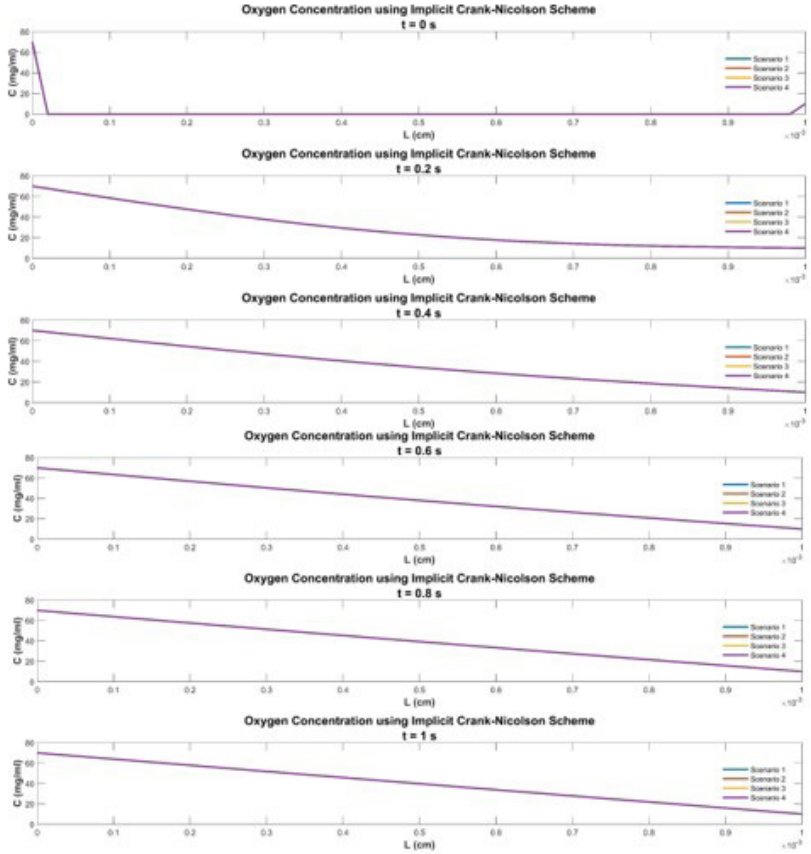

Figure 8 Simulation Results of Oxygen Diffusion with Crank-Nicolson Method in Scenario 1 to Scenario 4

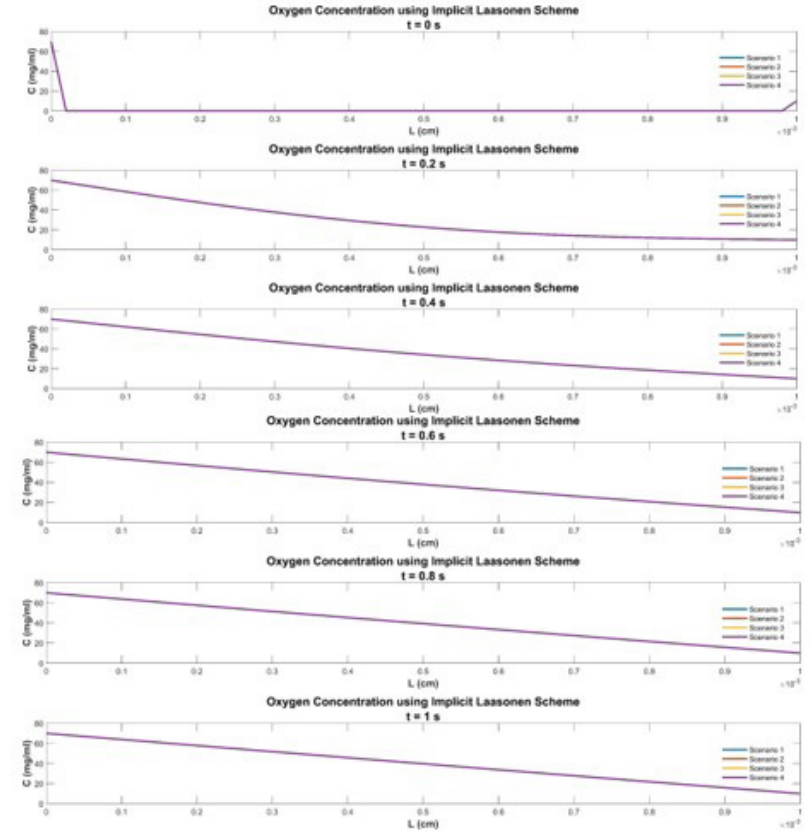

Figure 9 Simulation Results of Oxygen Diffusion with Laasonen Method in Scenario 1 to Scenario 4

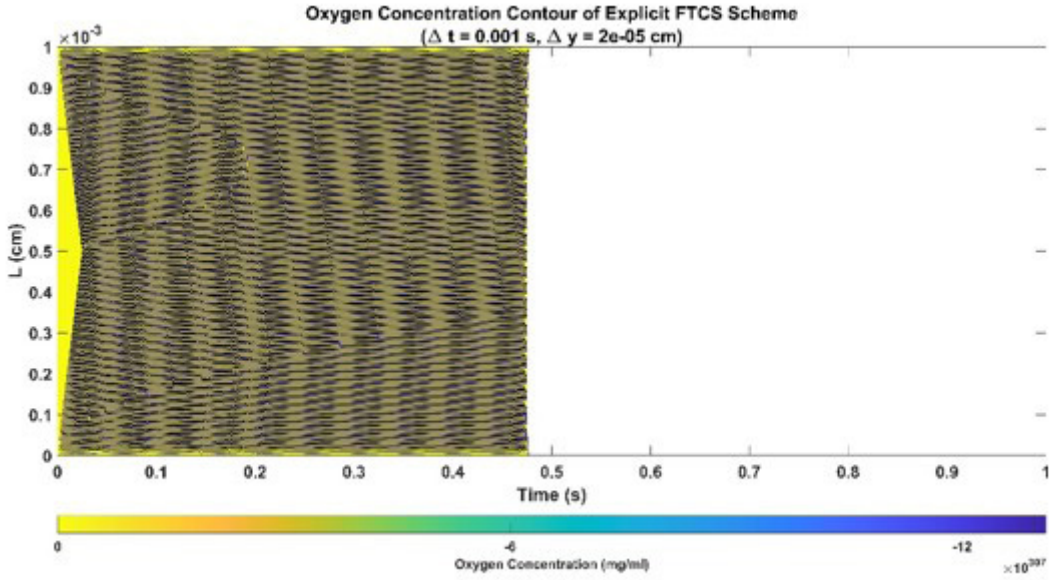

(A)

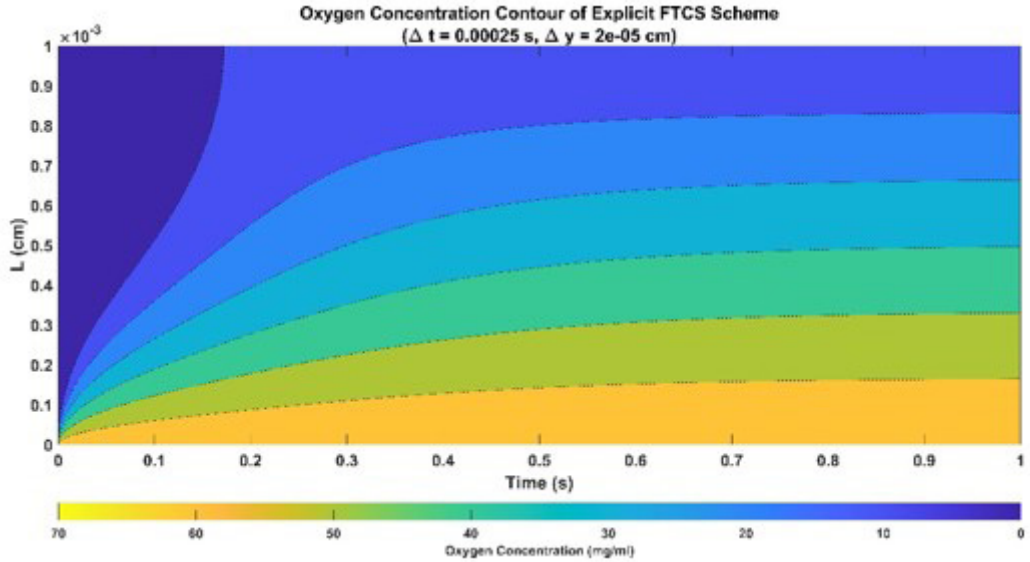

(B)

Figure 10 Oxygen Diffusion Contours Using the Explicit FTCS Method in Scenario 1 (A) and Scenario 4 (B)

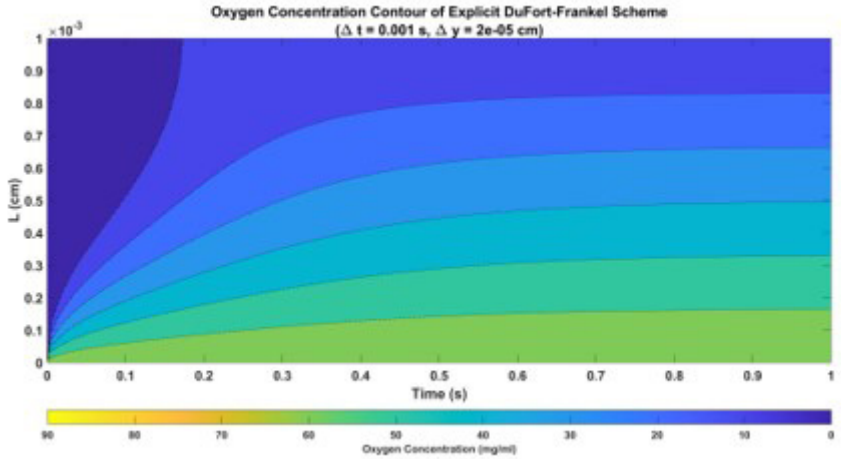

(A)

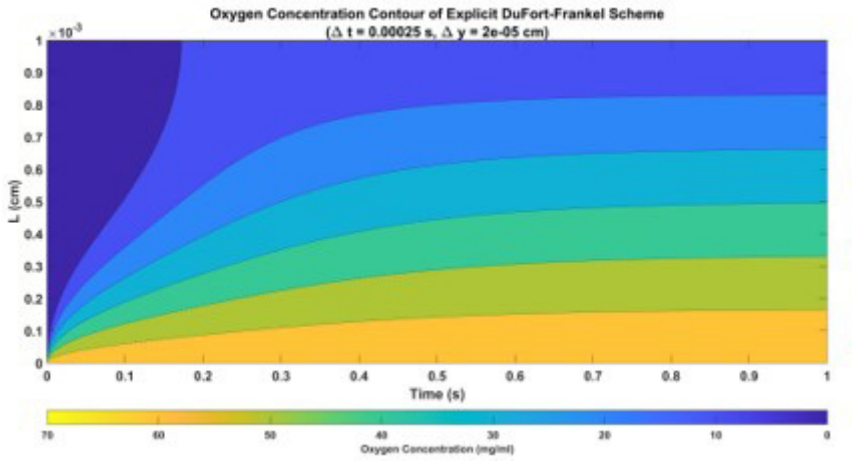

(B)

Figure 11 Oxygen Diffusion Contours Using the Explicit DuFort-Frankel Method in Scenario 1 (A) and Scenario 4 (B)

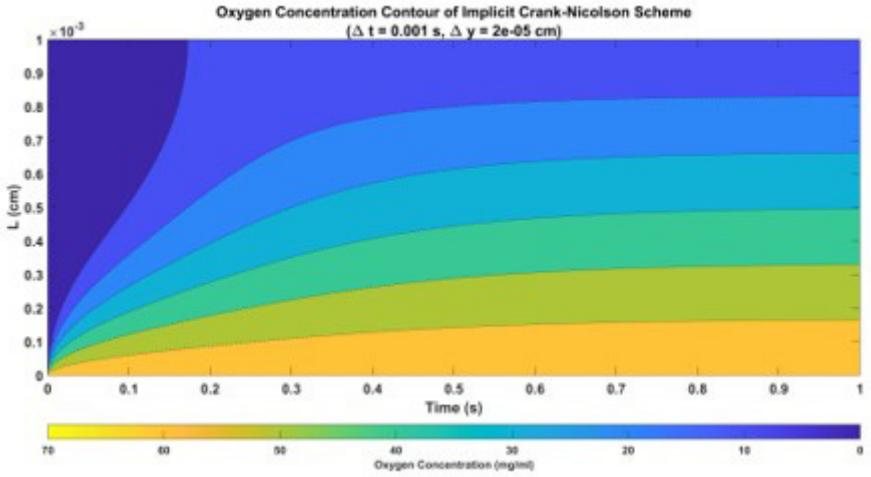

(A)

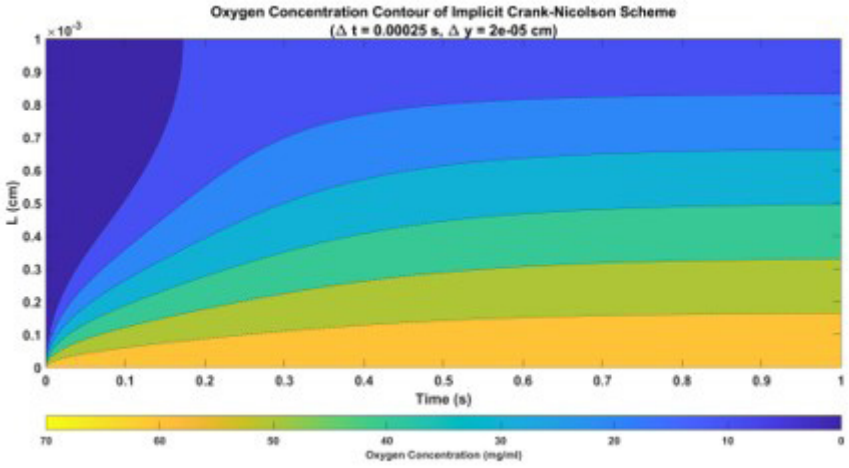

(B)

Figure 12 Oxygen Diffusion Contours Using the Implicit Crank-Nicolson method in Scenario 1 (A) and 4 (B)

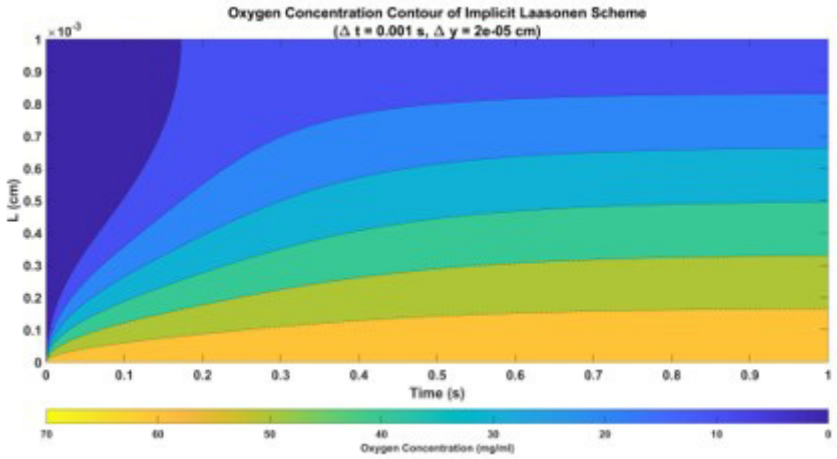

(A)

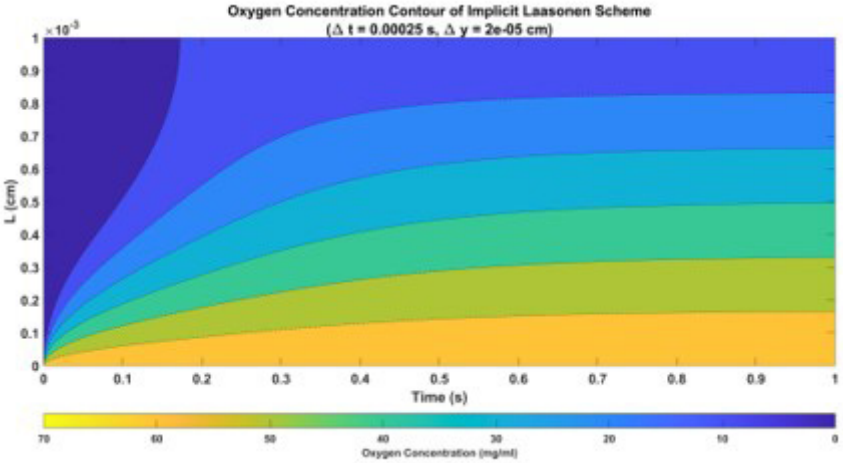

(B)

Figure 13 Oxygen Diffusion Contours Using the Implicit Laasonen Method in Scenario 1 (A) and Scenario 4 (B)

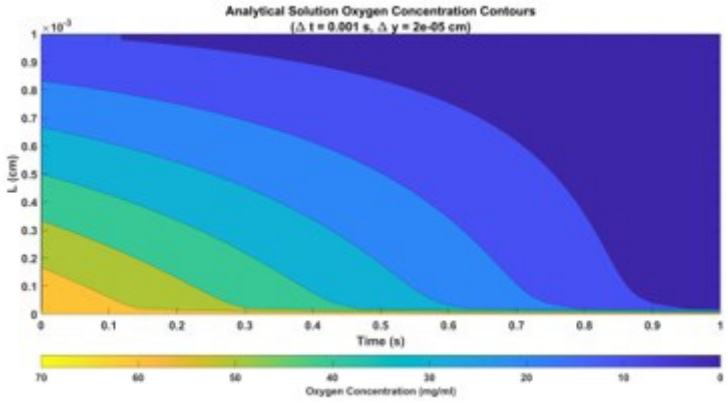

(A)

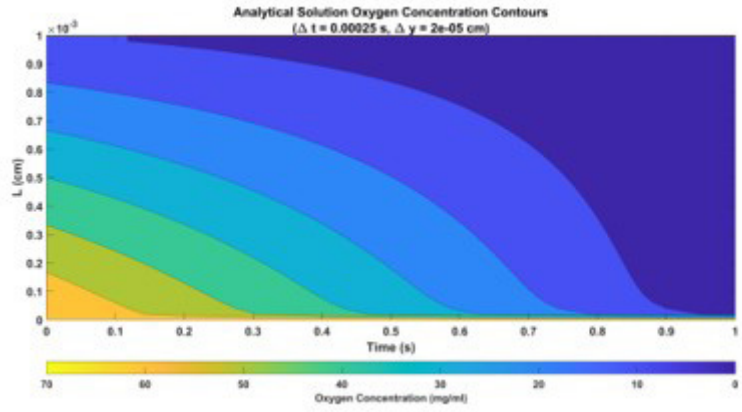

(B)

Figure 14 Oxygen Diffusion Contours Using the Analytic Solution of Δt = 0,0005 s (A) and Δt = 0,00025 s (B)

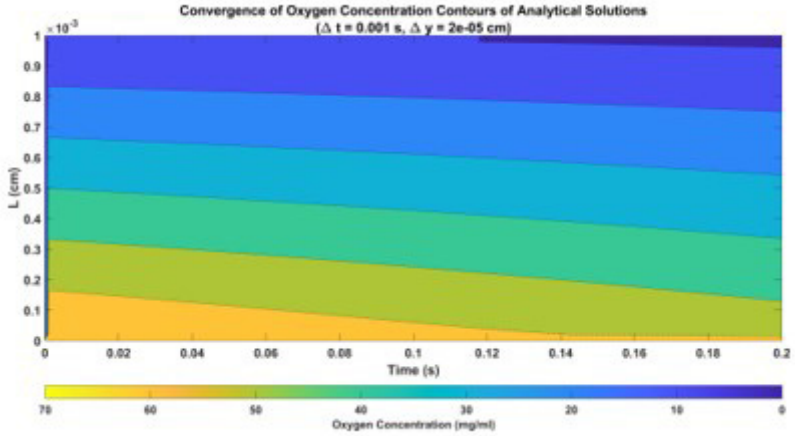

(A)

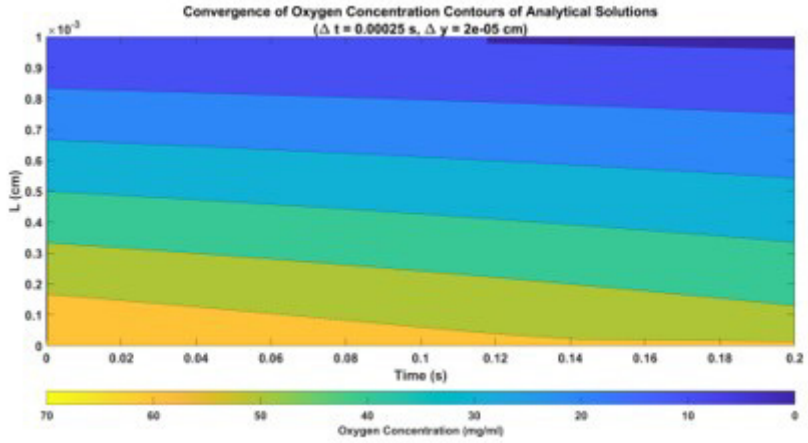

(B)

Figure 15 Convergence of Oxygen Diffusion Using Analytical Solutions of Δt = 0,0005 s (A) and Δt = 0,00025 s (B)

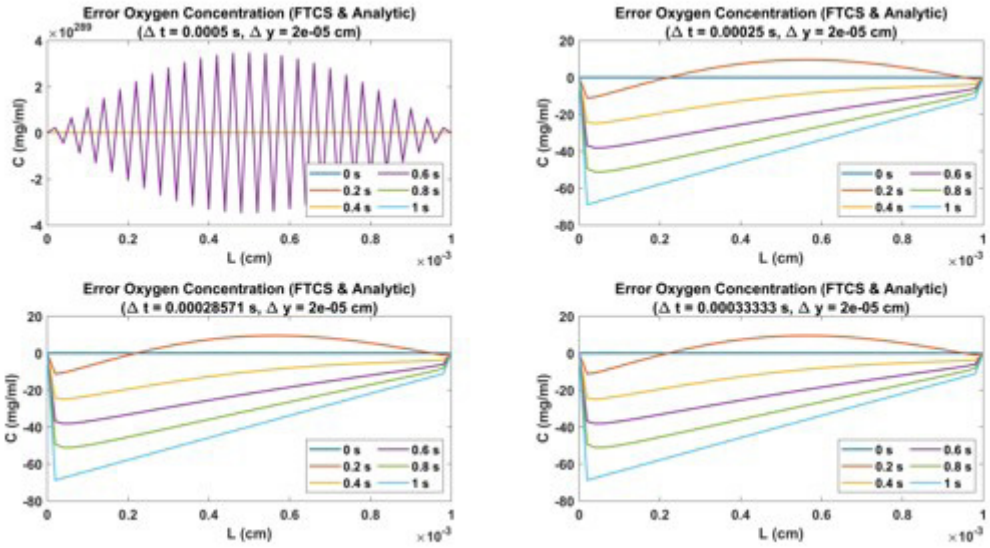
Error Oxygen Concentration (FTCS & Analytic)
(Δ t = 0.0005 s, Δ y = 2e-05 cm)
Error Oxygen Concentration (FTCS & Analytic)
(Δ t = 0.00025 s, Δ y = 2e-05 cm)
Error Oxygen Concentration (FTCS & Analytic)
(Δ t = 0.00028571 s, Δ y = 2e-05 cm)
Error Oxygen Concentration (FTCS & Analytic)
(Δ t = 0.00033333 s, Δ y = 2e-05 cm)
C (mg/ml)
L (cm)
0 s
0.2 s
0.4 s
0.6 s
0.8 s
1 s

(A)

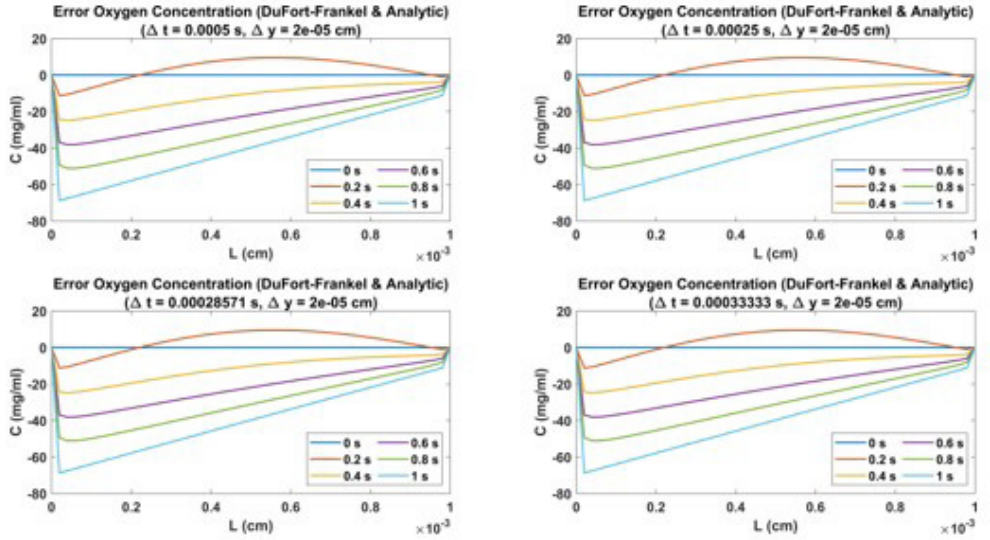
Error Oxygen Concentration (DuFort-Frankel & Analytic)
(Δ t = 0.0005 s, Δ y = 2e-05 cm)
Error Oxygen Concentration (DuFort-Frankel & Analytic)
(Δ t = 0.00025 s, Δ y = 2e-05 cm)
Error Oxygen Concentration (DuFort-Frankel & Analytic)
(Δ t = 0.00028571 s, Δ y = 2e-05 cm)
Error Oxygen Concentration (DuFort-Frankel & Analytic)
(Δ t = 0.00033333 s, Δ y = 2e-05 cm)
C (mg/ml)
L (cm)
0 s
0.2 s
0.4 s
0.6 s
0.8 s
1 s

(B)

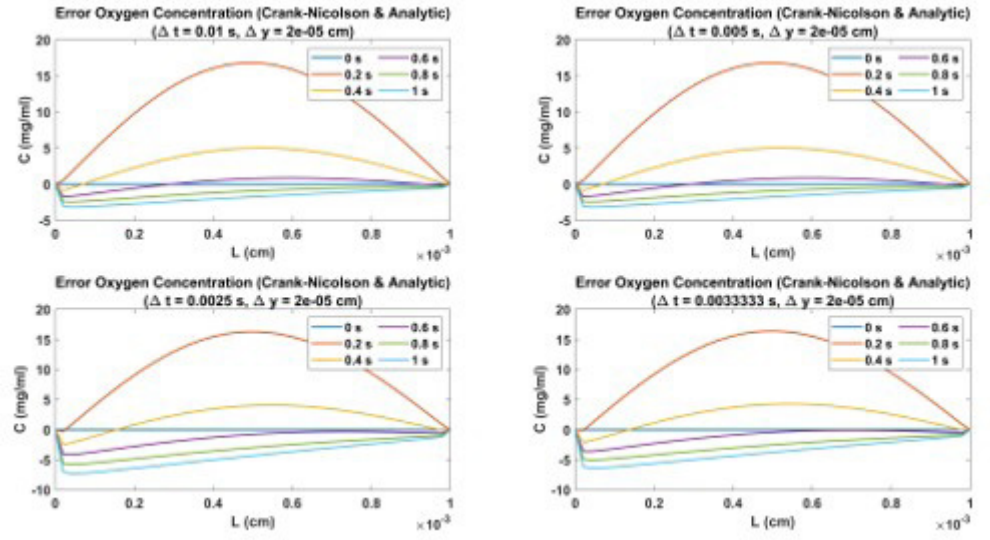
Error Oxygen Concentration (Crank-Nicolson & Analytic)
(Δ t = 0.01 s, Δ y = 2e-05 cm)
Error Oxygen Concentration (Crank-Nicolson & Analytic)
(Δ t = 0.005 s, Δ y = 2e-05 cm)
Error Oxygen Concentration (Crank-Nicolson & Analytic)
(Δ t = 0.0025 s, Δ y = 2e-05 cm)
Error Oxygen Concentration (Crank-Nicolson & Analytic)
(Δ t = 0.0033333 s, Δ y = 2e-05 cm)
C (mg/ml)
L (cm)
0 s
0.2 s
0.4 s
0.6 s
0.8 s
1 s

(C)

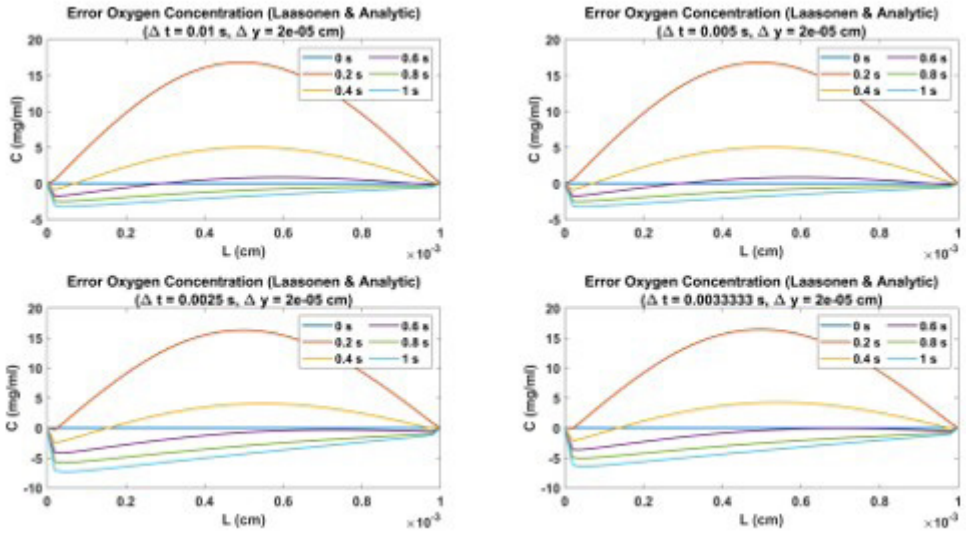

(D)

Figure 16 Error of Analytic Solution with Forward Time Center Space (FTCS) (A), DuFort-Frankel (B), Crank-Nicolson (C), and Laasonen (D) Models

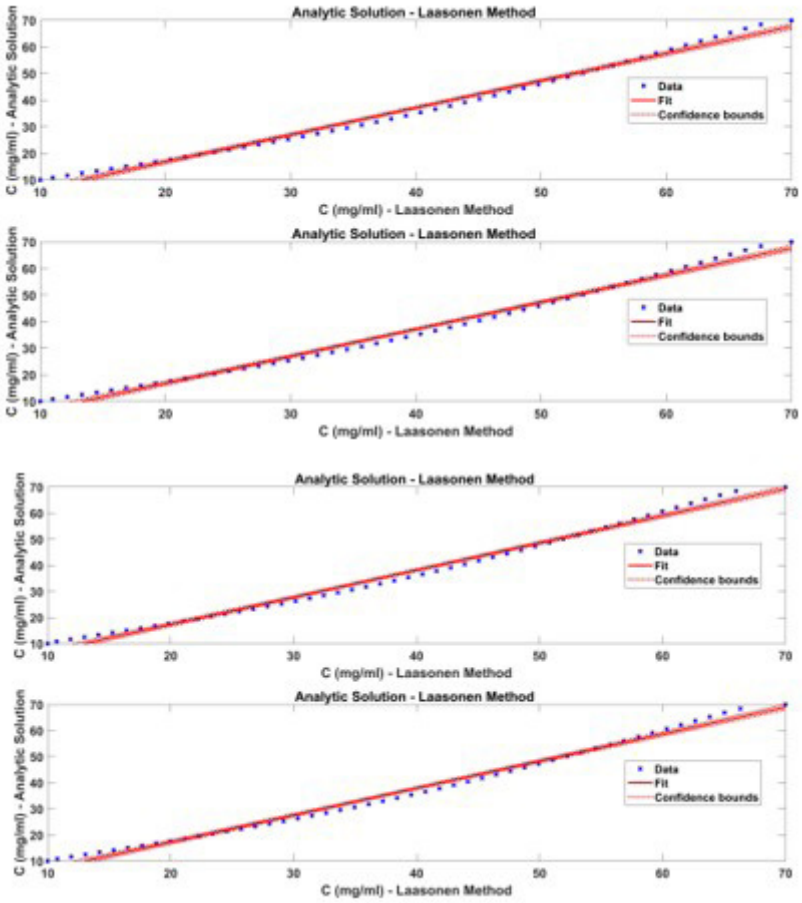

Figure 17 The Comparison of the Results of the Analytic Solution with the Laasonen Scheme